Possibility of an unequivocal test of different models of the equation of state of aluminum in the coupling regime $\Gamma \sim 1-50$

François Perrot
Centre d'Etudes de Bruyères Le Châtel, P. O. Box 12, 91689 Bruyères Le Châtel, France

M. W. C. Dharma-wardana*
National Research Council, Ottawa, Canada, K1A 0R6

John Benage
Los Alamos National Laboratory, Los Alamos, New Mexico, 87545

(Received 8 June 2001; published 3 April 2002)

The equation of state (EOS) in regimes of density (ρ) and temperature (T) which are inaccessible to experiment has to be determined using theories which may themselves be out of their range of validity. Even for Al, the EOS in the region $0.1<\rho<2$ g cm^{-3}, and $1<T<50$ eV, where the ionic coupling parameter Γ ranges from $1-\sim 50$, is not unknown. We present results for the EOS using the Thomas-Fermi model (TF), the quotidian equation of state, the Sesame tabulation, and using the density-functional neutral-pseudoatom (NPA) model which is a first-principles theory applicable at strong coupling. It is found that the NPA predictions are very different from the other models, and experiments could provide an unequivocal test of the validity of the different EOS models. We report theoretical results for the Hugoniot, and the electrical conductivity in the regime of interest.

DOI: 10.1103/PhysRevE.65.046414 PACS number(s): 52.27.Gr, 05.30.Fk, 71.10.−w, 71.45.Gm

I. INTRODUCTION

Building the equation of state (EOS) of materials requires the use of many physical theories, numerical methods, and experimental techniques. Even in presumably ''simple'' materials, the evaluation of thermodynamic properties may be very uncertain. The recent studies of dense deuterium, prompted by recent shock experiments done with the Nova laser, [1] prove that sound theoretical models, on which a lot of EOS data rely, may still be inadequate.

Aluminum is a simple metal, and is often considered an accurate standard for EOS studies. The knowledge of the aluminum EOS is good in the regime of the solid and the metallic liquid (i.e., for $\rho>2$ g cm^{-3}, and for temperatures up to a few electron volts), due to numerous static and dynamic measurements [2]. However, there are domains where no experimental information is available and common theories are out of their range of validity. This is true for very low and moderate densities, the temperature being not high enough to make the Thomas-Fermi statistical method reliable. The density/temperature plot of Fig. 1 illustrates the subregions covered by the theories used to calculate the Sesame EOS of Al [3]. The hatched area is not addressed by theory. It is accessed by numerical interpolation from the adjacent regions where data are available. The ''unknown'' area, roughly defined by, $0.1<\rho<2$ g cm^{-3}, $1<T<50$ eV, is such that the plasma is strongly coupled (the ionic coupling parameter $\Gamma=(Z^*e)^2/r_{ws}k_BT$, goes from 1 to 50). It will be called the $\Gamma(1-50)$ region. Here r_{ws} is the Wigner-Seitz radius such that the volume $V=4\pi r_s^3/3$, in atomic units, contains just one ion, i.e., $N=1$. An experimental technique, presently under development (e.g, at Los Alamos National Laboratory) probes the thermodynamics of dense plasmas in the $\Gamma(1-50)$ region [4]. An Al wire is heated to create a plasma which is allowed to expand, and then subject to a laser shock. The density and temperature behind the shock is expected to be of the order of 1 g cm^{-3}, and ~ 10 eV, respectively. The measurements give the density ρ, the pressure P, and the internal energy E. The objective of this study is to show that such experiments should be able to distinguish among the theoretical EOS models of dense plasmas in this regime, to well within experimental accuracies. We briefly present the theoretical models, the thermodynamic functions, and transport coefficients calculated from them. Examples of shock Hugoniot curves relevant to the ''unknown'' region are also given.

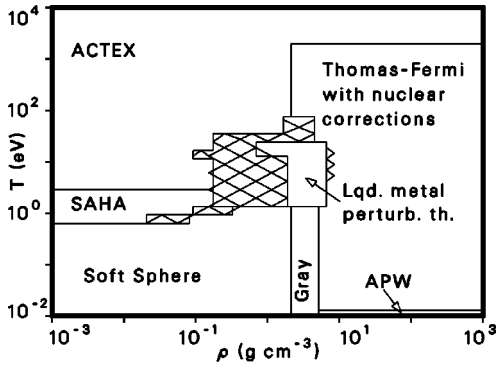

FIG. 1. Temperature-density plot of the subregions covered by various theories used to calculate the SESA equation of state for aluminum. The hatched $\Gamma(1-50)$ region is the object of the present calculation, using TF, QEOS, NPA, and an interpolation from the neighboring regions (SESA).

*Electronic address: chandre@cm1.phy.nrc.ca

II. EOS MODELS FOR ALUMINUM

We present four EOS models of aluminum dense plasmas. These models are: The genuine Thomas-Fermi (TF) model [5], the quotidian equation states (QEOS) model [6], the Sesame (SESA) model [3], and the neutral pseudoatom (NPA) model in the framework of density functional theory (DFT) [9], generalized to finite temperatures and constructed within a self-consistent treatment of ion correlations using the hypernetted-chain method inclusive of bridge corrections [7,8].

The Thomas-Fermi model (TF): The TF equation is solved accurately, and no analytical fits are used.

The QEOS model: This EOS, proposed by More *et al.*, pragmatically tries to correct for the most important shortcomings of the TF model. The free energy of the material is written as:

$$F(V,T)=E_b(V)+[F_{TF}(V,T)-F_{FT}(V,0)]+F_i(V,T).$$

$E_b(V)$ is a binding energy at $T=0$ substituted for the TF energy. The thermal part of the electronic free energy remains that of the TF model without any quantum corrections. An excess-ionic contribution $F_i(V,T)$ is included. In the solid phase, $F_i(V,T)$ is given by the Debye model with a Debye temperature T_D depending on the density according to parametrized forms due to Cowan. The parameters are chosen to fit the experimental T_D, the Grüneisen coefficient γ, and the melting temperature T_m at normal density. Those two are related by the Lindemann law. In the fluid phase, $F_i(V,T)$ interpolates between the Dulong-Petit solid at $T_m(V)$ and the perfect ideal gas at very high temperature, with a scaling in $T_m(V)/T$. A calculation of the electrical resistivity within the same conceptual and phenomenological framework as the QEOS is available via the work of Lee and More [10].

The Sesame (SESA) EOS: The Sesame library, developed at Los Alamos National Laboratory, is widely used for numerical simulations. In the $\Gamma(1-50)$ region, SESA is an interpolation between the results of several theories valid in adjacent domains. These theories are: (i) higher densities; liquid-metal perturbation theory with electronic excitations up to about $T=20$ eV, and TF theory with electronic quantum corrections and ionic corrections for T above 20 eV, (ii) lower densities; Saha model to approximately $T=3$ eV, and then an activity expansion (ACTEX) based on static-screened potentials is used for higher temperatures [11].

The Neutral Pseudo Atom (NPA) model: The NPA model was first proposed for solid simple metals at $T=0$ [9]. The problem of the ion distribution does not arise in solids. A self-consistent density-functional theory of the ion distribution coupled to the electron distribution leads to a liquid-metal type theory of the EOS of a plasma within the so-called ''physical picture,'' i.e., a first-principles theory [7,8]. It combines an average-atom full self consistent Kohn-Sham treatment of the electrons, both bound and free, with a description of the ionic fluid using the classical theory of liquids (this is in fact a classical DFT for ions). For the electrons, the Kohn-Sham-Mermin [12] equations are solved for a single ''pseudoatom'' embedded in a jellium with a cavity. A temperature-dependent exchange and correlation potential, as parametrized in Iyetomi and Ichimaru [13] is added to the Hartree potential. The displaced electron charge density around the nucleus consists of a localized bound contribution $n_b(r)$ and a free delocalized contribution $n_f(r)$. The uniform density of the jellium in which the atom is embedded is self-consistently determined from these densities. It is related to the average ionization Z^* by: $Z^*\rho=n$, in atomic units. The free energy required to embed the atom in the jellium, $F_I(V,T)$, is also calculated from the Kohn-Sham wave functions. Assuming that the density response function of the metal is similar to that of a uniform electron gas at the density n and at temperature T, a pseudopotential is determined which reproduces the self-consistent free-electron charge density $n_f(r)$. With this pseudopotential, the ion-ion interaction is computed. A hyper-netted-chain equation inclusive of a bridge function is solved for the pair-correlation function [14], from which the ionic free energy $F_{12}(V,T)$ is calculated. Finally, the total free energy of a plasma atom is

$$F(V,T)=Z^*f(V,T)+F_I(V,T)+F_{12}(V,T). \tag{1}$$

Here $f(V,T)$ is the free energy of an electron in a uniform interacting electron gas of density n at temperature T. Variational properties of the free energy may be used to simplify the calculation of the internal energy and pressure. This approach is accurate for $T>5$ eV. At lower temperatures, taking account of several multiply charged ions instead of an average atom becomes necessary [8]. At still lower temperatures, molecules and clusters arise and require multicenter DFT calculations.

Once the basic properties of the plasma [i.e., Z^*, electron-ion interaction V_{ei} and the structure factor $S(k)$] are obtained, the transport coefficients, e.g., the resistivity [8], and the energy-relaxation coefficient [15], etc., may be evaluated.

III. NUMERICAL RESULTS AND COMPARISONS

The main differences between the NPA and the TF-type models arise from the inclusion of finite-sized, compressible, interacting discrete ions within the associated ionization equilibrium. Also, an explicit treatment of the continuum lowering due to electron-electron exchange correlation, and electron-ion correlation, gets included in the NPA. We present results for the excess internal energy E_{ex}, excess pressure P_{ex}, and the electrical resistivity R, calculated within the different EOS models.

$$E_{ex}=E-(3/2)k_BT, \tag{2}$$

$$P_{ex}=P-k_BT/V. \tag{3}$$

Note that the number of particles N in the volume $V=4\pi r_{ws}^3/3$, is one. The electrical conductivity within the QEOS is evaluated using the approach due to Lee and More, while that from the NPA is given in Ref. [8].

We use the results of thermodynamic calculations for the QEOS and SESA models done by Renard [16]. Some tabulations of the thermodynamic functions for our NPA model,

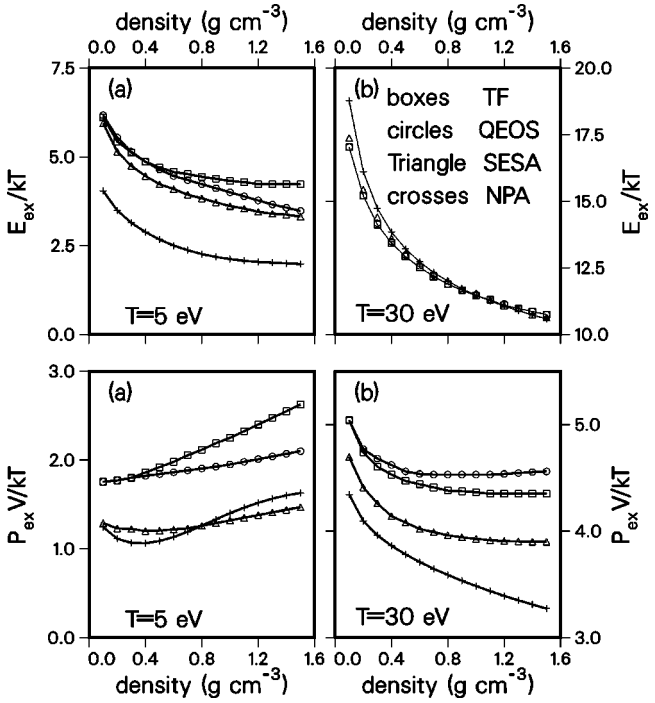

FIG. 2. Two upper panels: excess internal energy, E_{ex}/Nk_BT, with V such that $N=1$, is given as a function of density in the four EOS models, for $T=5=30$ eV. Two lower panels: excess pressure, $P_{ex}V/Nk_BT$, with $N=1$, as a function of density $T=5$ and 20 eV.

as well as the code for carrying out such calculations via on-line input, are given at our website [17].

The variation of the excess internal energy E_{ex}/Nk_BT, with $N=1$, for densities ranging from 0.1 to 1.5 g cm^{-3}, and temperatures k_BT = 5, 10, 15, 20, 25, and 30 eV is considered (for detailed tabulations, see [17]). Figure 2 displays the k_BT = 5 and 30 eV data. The behavior is rather similar for the TF, QEOS, and SESA energies, while there is a significantly different behavior for NPA. The excess energy is smaller by a factor of about 2 at low temperature; its density variation is steeper for the lowest densities, and the temperature gradient is weaker at low temperature but stronger at higher temperature. The *magnitude* of E_{ex}/k_BT depends on the chosen energy origin, which is the energy of the isolated Al atom (-482.6705 Ry for NPA). These differences are easily seen in the specific heat, shown in Table I.

Figure 2 shows $P_{ex}V/Nk_BT$, with $N=1$, as a function of ρ for the two values of T. Note that ideal-gas term $P_0V/k_BT=1$ and only the excess component is displayed. For more results, see [17]. The P_{ex} in NPA has two components, viz., from electrons and from screened ions. The TF-type models have no explicit treatment of the ions. The results for TF and QEOS are very similar at $T=30$ eV, while SESA shows the same density variation as TF at a lower pressure. NPA is different from the other three EOS; the pressure is always lower, and its density variation is larger. This would result in a very different sound velocity. At $T=30$ eV, all curves show a decrease of $P_{ex}V/k_BT$ with increase of density (N.B. $P_{ex}V/k_BT$ is a decreasing function of the density even if P_{ex} were constant. Moreover, the derivative of the total pressure, $\partial P/\partial V|_T$ is negative as it should be). This behavior is most pronounced in the NPA, and is a result of the interplay betwen the density, ionization balance, the compressibility of the screened ions and the electron pressure. Also, the NPA model admits a realistic treatment of the reduction in fugacity due to electron-electron exchange and correlation, ion-electron, and ion-ion correlations, while the other models do not explicitly address such effects.

TABLE I. Specific heat $[\partial E_{ex}/\partial(k_BT)]_V$ in the SESA and NPA models.

ρ g cm^{-3}	SESA	NPA	SESA	NPA
T (eV)→	5	5	30	30
0.1	12.9	9.4	25.6	36.3
1.5	7.9	5.0	15.7	19.6

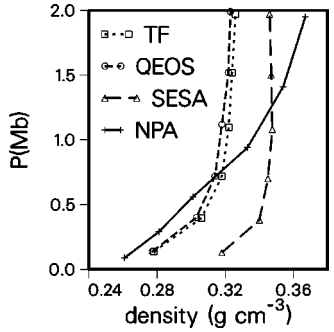

FIG. 3. Hugoniot curves for initial conditions $\rho_0=0.05$ g cm^{-3} and $k_BT_0=1.0$ eV, as calculated in the four EOS models.

A. Hugoniot curve for a typical experiment

In the proposed experiments (referred to in the introduction) a shock is induced in the Al plasma with an initial density much lower than the solid density, and the shock pressure is in the megabar range. We have calculated the Hugoniot curves for such shocks using the four EOS. The initial density is $\rho_0=0.05$ g cm^{-3} and the temperature is $k_BT_0=1$ eV. The four curves are shown in Fig. 3. The thermodynamic functions in the initial state are not known. We have checked that the use of some plausible values for the initial internal energy, E_{in}, and the pressure, P_{in}, does not influence the density and pressure behind the shock above 0.4 Mb. So, for the initial state of the shock, we have taken E_{in} and P_{in} to be that of the perfect gas at ρ_0 and T_0 (We emphasize that some other choice, e.g., $P_{in}=E_{in}=0$ would not affect the Hugoniots above 0.4 Mb). The TF and QEOS curves are too close for experimental discrimination. But the SESA and NPA curves are very different from the previous ones, and between themselves: the SESA is much steeper, with an asymptotic density $\rho=0.35$ g cm^{-3}. With the DFT-NPA, ρ does not saturate for pressures up to 2 Mb. At $P=0.5$ Mb, the SESA and NPA densities differ by 15%. We

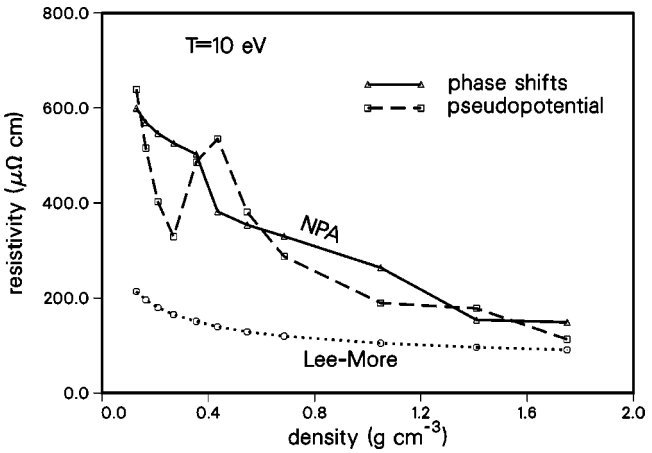

FIG. 4. Electrical resistivity for a typical system at $T=10$ eV calculated from the Lee and More model, and from the DFT-NPA model. In the NPA case the resistivity is evaluated from the pseudopotential constructed from the NPA-charge density, and from the scattering phase shifts.

believe that typical experimental accuracies are quite sufficient to determine which of the EOS models best describes the experiments.

The NPA model ''absorbs'' a large change in matter density for the range of pressures shown in Fig. 3. In some sense, this is because the change in internal volume of the atom (associated with changes in Z^*) and the screening cloud allows this gradual density change. In fact, a similar effect is seen in Fig. 4, where a larger change in resistivity occurs over the density range shown (unlike in the TF model of Lee and More where R versus ρ is ''flat,'' because here also Z^*, the free-electron density, and the ion distribution come in to play.

B. Electrical resistivity

In Fig. 4 we show the electrical resistivity for a typical case within the region studied. The Lee-More Thomas-Fermi-type approach, does not show the structure shown by the NPA calculation. The Ziman formula is used, with the electron-ion interaction described by (a) the pseudopotential (constructed from the NPA charge density), (b) a scattering amplitude constructed from the phase shifts of the pseuodoatom. A detailed discussion of various models of resistivity within the NPA scheme has been given in Ref. [18]. The structure in the NPA resistivity arises from the transition of Z^* from ~ 2 in the low-density regime, to $Z^* \sim 3$ in the high-density regime. These results show that measurements of the electrical resistivity would also serve to distinguish between the various available plasma models.

IV. CONCLUSION

We have reported results on the aluminum EOS and transport properties in the regime of dense strongly coupled plasma obtained from several models, one of which is a first-principles model. These results show important differences in the thermodynamic functions, with drastic consequences on the pressure of shocks that can be induced in plasmas initially obtained by electrical heating followed by expansion. The predicted transport properties also show clear differences between the NPA and the Thomas-Fermi-type models. In our opinion, the existence of large differences in theoretical predictions should be a strong motivation for experiments which are potentially able to discriminate among available models of hot dense matter.

[1] L.B. Da Silva, P. Celliers, G.W. Collins, K.S. Budil, N.C. Holmes, T.W. Barbee, B.A. Hammel, J.D. Kilkenny, R.J. Wallace, M. Ross, R. Cauble, A. Ng, and G. Chiu, Phys. Rev. Lett. **78**, 483 (1997).

[2] B.L. Glushak, A.P. Zharkov, M.V. Zhernokletov, V.Y. Temovdf, A.S. Filimonov, and V.E. Fortov, Zh. Éksp. Teor. Fiz. **96**, 1301 (1989) [Sov. Phys. JETP **69**, 739 (1989)]; M. V. Zhernokletov, V. N. Zubarev, R.F. Trunin, R. F. Trunin, and V. E. Fortov, *Experimental data on shock compressibility and adiabatic expansion of condensed materials at high densities* (Russian Academy of Sciences, Chernogolovska, 1996) (in Russian).

[3] K. Trainor, in *Handbook of Material Properties Data Bases*, edited by W. Huebner (Los Alamos National Laboratory, Los Alamos, 1984), Vol Ic, p. 3712.

[4] J. F. Benage, G. Kyrala, J. Workman, and T. Tierney, *Strongly Coupled Coulomb Systems*, edited by G. Kalman (Plenum, New York, 1998).

[5] R. Latter, Phys. Rev. **75**, 1854 (1955).

[6] R.M. More, K.H. Warren, D.A. Young, and G.B. Zimmerman, Phys. Fluids **31**, 3059 (1988).

[7] F. Perrot, Phys. Rev. E **47**, 570 (1993).

[8] F. Perrot and M.W.C. Dharma-wardana, Phys. Rev. E **52**, 5352 (1995).

[9] L.J. Dagens, J. Phys. (Paris) **34**, 879 (1973).

[10] Y.T. Lee and R.M. More, Phys. Fluids, **27**, 1273 (1984).

[11] F.J. Rogers, Phys. Rev. A **24**, 1531 (1981).

[12] W. Kohn and L.J. Sham, Phys. Rev. **140**, A1133 (1965), N.D. Mermin, Phys. Rev. A **137**, 1441 (1965).

[13] H. Iyetomi and S. Ichimaru, Phys. Rev. A **34**, 433 (1986); use of a more recent V_xc, e.g., F. Perrot and M.W.C. Dharma-wardana, Phys. Rev. B **62**, 16536 (2000) gives changes which do not modify the main conclusions.

[14] F. Lado, S.M. Foiles, and N.W. Ashcroft, Phys. Rev. A **28**, 2374 (1983).

[15] M.W.C. Dharma-wardana and F. Perrot, Phys. Rev. E **58**, 3705 (1998).

[16] F. Renard (unpublished).

[17] http://nrcphy1.phy.nrc.ca/ims/qp/chandre/Al_eos/

[18] François Perrot and M.W.C. Dharma-wardana, Int. J. Thermophys. **20**, 1299 (1999).